Journal Name

View Article Online
Dynamic Article Links

Cite this: DOI: 10.1039/c0xx00000x

www.rsc.org/xxxxxx

ARTICLE TYPE

Structure *vs* properties -chirality, optics and shapes- in amphihilic porphyrin J-aggregates

Zoubir El-Hachemi,[a] Carlos Escudero,[b] Francisco Acosta-Reyes,[c] M. Teresa Casas,[c] Virginia Altoe,[d] Shaul Aloni,[e] Gerard Oncins,[f] Alessandro Sorrenti,[a] Joaquim Crusats,[a] J. Lourdes Campos,[c] Josep M. Ribó*[a]

Received (in XXX, XXX) Xth XXXXXXXXX 20XX, Accepted Xth XXXXXXXXX 20XX
DOI: 10.1039/b000000x

The structure of the *meso*-tetrakis(4-sulfonatophenyl)porphyrin ($TPPS_4$) J-aggregates could be determined by X-ray and electron diffraction methods. A sheet-like architecture reveals the relationship between structure and chirality, optics and shapes of the J-aggregate of the *meso* 4-sulfonatophenyl- and phenyl-substituted porphyrins. The structure of the J-aggregates of H_4TPPS_4 belongs to the chiral space group $P2_1$ and includes four porphyrin molecules in its unit cell. The intermolecular stabilization of the zwitterionic units by hydrogen bonding and electrostatic interactions between the positively charged central NH groups and the periphery anionic sulfonato groups results in a structure of porphyrins sheets along the $[101]$ plane direction. The structure of the sheet on the $[\bar{1}01]$ plane is already chiral and its molecular architecture explains the simultaneous presence of H- and J-aggregate bands in their absorption spectra. This structure also accounts for the high similarity observed between the absorption spectra of different mesomorphs of the same substance and even between different members of the series of *meso*-4-sulfonatophenyl-and-aryl substituted diprotonated porphyrins. The possibility, or not, of the sheet-like structure on $[101]$ to interact with other layers, either through ionic or hydrophobic interactions, depends on the substitution pattern at the *meso*-positions of the porphyrin ring. Thus, the different morphologies of the particles [mono- bi- and multilayered] of this series of J-aggregates are explained taking into account the role that the fourth *meso*-subtituent plays in the interlayer stabilization. The results suggest that supramolecular helicity, previously detected in several J-aggregates, is not the explanation of their chirality but would be the expression of the intrinsic chirality of the packing between building blocks.

1. Introduction

J-aggregates, for example those of cyanines and porphyrinoids, show optical and photochemical properties of significant interest not only in supramolecular chemistry and materials science,[1] but also in biological chemistry because of their relationship with the architecture of the pigment aggregates which form the natural light-harvesting antennas in green plants.[2]

meso-4-Sulfonatophenyl-and-aryl-substituted porphyrins (Scheme 1) are amphiphilic porphyrins, which in acidic media form J-aggregates as nano- or microparticles in suspension. Their aggregation processes are based on a hierarchical self-assemblies showing different thermodynamic and kinetically controlled paths.[3] In this respect, they show analogies with other J-aggregates, for example with the J-aggregates of cyanine dyes, but in the case of porphyrins their formation occurs at lower concentrations and does not lead to viscous phases thus making the assessment of their optical properties much easier.

Previous results on the relationship between the structure and the optical properties (electronic spectra and optical polarization) of these porphyrin J-aggregates raise several questions, which are summarized in what follows.

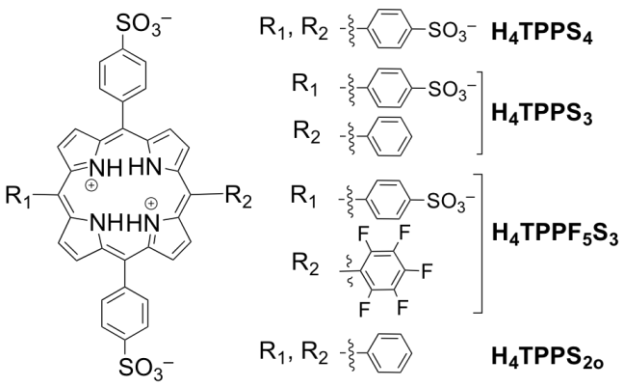

Scheme 1. Formula Scheme.

1.1. Structure *vs* excitonic spectra

J-aggregates are a paradigm of how the electronic structure of a building block can be modified as a result of its self-assembly into supramolecular species. In the case of the porphyrins in Scheme 1, the Soret (≈ 434 nm) and Q (≈ 644 nm) bands of the porphyrin are red-shifted, ≈ 489 nm and ≈ 705 nm respectively, as a consequence of the coupling of transition dipoles (side-to-side arrangements <=> J-aggregates) forming extended domains of excited states, as detected by resonance light scattering (RLS). The J-excitonic bands are composed by degenerate, or quasi-degenerate, transitions as evidenced by the bisignated character of the bands in their circular dichroism (CD) spectra. In this respect, it is surely significant that the decomposition of the J-band into two transitions has been also observed in other types of J-aggregates.[4] An unclear point is whether or not the origin of a blue-shifted Soret band (≈ 420 nm) is the consequence of π-stacking interactions (face-to-face <=> H-aggregates) between the chromophores. Some authors had attributed this H-band to independent species of H-aggregates. However, polarized fluorescence spectra of H_4TPPS_4 J-aggregate solutions[5] as well linear dichroism measurements[6] show the orthogonal arrangement of H- (≈ 420 nm) and J-transitions (≈ 490 nm), i.e. that both excitons are forming part of the same structure.

In summary, a reasonable structure of the title J-aggregates should take into account the presence of orthogonal H- and J-excitonic bands and the presence of degenerated excitonic bands.

1.2. The molecular chirality *vs* supramolecular chirality question

A significant characteristic of the J-aggregates of the porphyrins of Scheme 1 is that, depending on the experimental conditions during their preparation, they show natural optical activity. The CD signals cannot be attributed to artifactual combinations of linear polarizations because similar bisignated CD signals showing the same pattern are also detected for small round particles of the aggregates, which certainly do not originate linear polarizations. Furthermore, in the case of long-shaped particles of the aggregates the use of two-photomodulators polarimetry and Mueller-matrix methods allowed to discriminate between combinations of linear polarizations and true CD in the experimental CD signals.[7] In fact, recent results suggest that the title J-aggregates do have chiral structures[6] and that the detection, or not, of optical activity in samples would depend on whether scalemic or racemic mixtures are finally obtained. This is analog to the case in which achiral compounds form enantiopure crystals as the most stable mesomorph, yielding the racemic mixture of chiral crystals called racemic conglomerates. In such crystallizations high enantiomeric excesses may be obtained by the enantioselective growth of an Adam crystal formed in the primary nucleation stage.[8] This can be either achieved by a slow crystal growth[8a] or by the enhancement of the secondary nucleation processes.[8b-d]

The formation of the title J-aggregates can be considered to be a non-covalent polymerization process that shows a cooperative effect after a critical nucleation that drives the aggregation.[9,10] The primary nucleation would correspond to the initial stage before the cooperative effect operates and, the secondary nucleation, to the subsequent growth of these first nuclei of J-aggregates. The secondary nucleation may lead to different mesomorphs either through kinetically or thermodynamically controlled mechanisms (see examples in refs.[3]). In this respect, the diastereo and enantioselective growth of $H_4TPF_5S_3$ J-aggregates under the action of laminar flows, originated as a consequence of imperfect mixing, have been recently reported.[10,11] In fact, the enantioselective control of the first critical chiral nuclei is already implicit in the reports describing the phenomenon of chiral sign selection by the effect of the swirling direction of stirring vortices during the formation of H_4TPPS_3 J-aggregates.[12]

Presumably, other types of J-aggregates also form intrinsically chiral structures. In this respect, CD signals have been detected for the J-aggregates of achiral dyes of cyanine type.[1b,13] Notice that in previous reports on the detection of optical activity in several J-aggregates by the induction with chiral dopants, the chiral structures were attributed to be the result of the direct induction by the chiral additive on the final structures. However, in the light of recent reports it is reasonable to assume that most J-aggregates do actually form racemic conglomerates and that the chiral induction at the critical nucleation stage is in fact what biases the process towards a final scalemic mixture.

In summary, the structures of the title J-aggregates show chiral excitonic absorptions and this necessarily implies the existence of an intrinsically chiral structure. ‡,[14]

1.3. The question on the similar absorption spectra of different mesomorphs and J-aggregates of isomeric porphyrins

An intriguing point is that, in spite of having a different *meso*-substitution pattern, all porphyrins depicted in Scheme 1 for J-aggregates whose excitonic spectra do not show significant differences, not even between different mesomorphs (≈ 700 nm, ≈ 490 nm and ≈ 420 nm; monomer absorption ≈ 434 nm). For example, similar spectra are obtained for: a) H_4TPPS_4 J-aggregates consisting of nanotubes[15] compared to the common compact structures;[3,5] b) monolayers and bilayers of the steroisomeric H_4TPPS_3 and $H_4TPPF_5S_4$ J-aggregates.[11,12b] Furthermore, it is surely significant that the J-aggregates of 4-carboxyphenyl and 4-phosphonatophenyl *meso*-substituted porphyrin analogues show an absorption spectra pattern similar to that of H_4TPPS_n.[16,17]

In summary, the basic structural architecture responsible for the excitonic spectra must be shared by the different J-aggregates of the porphyrins in Scheme 1. Furthermore, this unique architectural trend must already appear during the critical primary nucleation stage, because the absorption spectra of the aggregates, at the different stages of the hierarchical self-assembly process, are alike.

1.4 Methodology

In this paper we determine the structure of the J-aggregates of H_4TPPS_4 by combining X-ray diffraction obtained from a thin film of a large well-aligned aggregate assembly and from electron diffraction data of individual nanofibrils. In this way we are able to overcome the unavailability of macroscopic single crystals and the sensitivity of the nanofibrils to the electron beam damage that make the determination of their crystal structure impossible.

2. Materials and methods

Absorption spectra were performed in a Cary/Varian 500Scan spectrophotometer. Resonance light scattering (RLS) measurements of $H_4TPPF_5S_3$ at the first stages of the aggregation were performed in synchronic mode in a PTI spectrofluorimeter.

2.1. Porphyrins and J-aggregate samples

Porphyrin synthesis, purification, and analysis were performed as previously described.[5b,18] Batch samples were assessed by HPLC analysis for the presence of significant amount of byproducts[18a] that could interfere in the homoassociation due to the formation of heteroaggregates. In the case of H_4TPPS_4 obtained by sulfonation of H_2TPP, the presence of 5-(3-sulfonatophenyl)-10,15,20-tris(4-sulfonatophenyl)porphyrin was lower than 0.5 %.

The preparation of H_4TPPS_4 J-aggregates by acidification of the tetrasodium salt of the free base porphyrin implies the segregation of the sodium salt as halite crystals,[18a] which could interfere in the preparation and analysis of the aligned sample. Therefore, the starting H_4TPPS_4 J-aggregate solutions for the X-ray diffraction measurements correspond to the acid species[18] of H_2TPPS_4 ($\approx$ 4 mM) at a pH value of $\approx$ 2 (adjusted by the addition of a small amount of sulfuric acid); see in the Results and Discussion section the effect that the pH value has in the aggregation. At these high porphyrin concentrations long compact tape-like structures were obtained, as observed by AFM in tapping mode.

2.2. Atomic force microscopy (AFM)

AFM measurements were performed in a Multimode 8 AFM attached to a Nanoscope V electronics (Bruker). The AFM probes had triangular-shaped silicon nitride cantilevers with silicon oxide tips to enhance resolution (SNL-10 probes, Bruker). AFM images were acquired at 1 Hz and 512x512 pixels. The topographic measurements were obtained in Peak Force mode. Briefly, this mode performs force curves at 2 kHz on the sample surface while using a set point deflection as the feedback signal. This mode enables to track the topography of the sample while applying vertical force values in the range of 100 pN -200 pN. The thickness of J-aggregates previously reported using older instruments were measured again using the instrument and experimental procedure described above. The samples of the J-aggregates studied here show by AFM in tapping mode long compact tape-like particles, which were 3 µm - 500 nm long, 50 nm -70 nm wide, and had a 3.8 nm thickness (see Supporting Information), together with a significant amount of much smaller particles.

2.3. Diffraction Methods

2.3.1. X-ray

The H_4TPPS_4 J-aggregate solution was oriented by slowly sliding it on the surface of a Teflon tube during the drying process under P_2O_5. Notice that this procedure implies Ostwald ripening, i.e. the formation of thicker long particles (> 3.8 nm; multilayered particles with 1.8 nm – 1.9 nm steps) at expenses of the smaller particles of J-aggregates. The oriented film was then carefully separated and fixed on a capillary in the parallel direction to that of its orientation; the X-ray beam was perpendicular to the direction of the orientation. Notice that the X-ray diffraction data corresponds to a mixture of micro/nano particles preferently aligned in one direction.

Diffraction images were acquired with a modified Statton camera (W. R. Warhus, Wilmington, DE) with Ni filter and Cu radiation (0.1542 nm wavelength).

An example of the X-ray diffraction pattern is shown in Fig. 1. The outside ring is due to a Silicon powder (011) standard (Natl. Bur. Stand. USA). Owing to the high inclination of the film, most of the equatorial reflections are only found at one side of the pattern. The distances corresponding to all determined *h*,*k*,l parameters are reported in the Supporting Information.

2.3.1.2. Optimization of porphyrin packing in the unit cell. The H_4TPPS_4 initial geometry was obtained from Gaussian-3 calculations [UHF, 6-311G(d) basis][19] which yield a S_4 symmetry and a distance between opposite sulfonato groups (O to O) of 19.75 Å. To improve the hydrophobic interactions in the zwitterion stabilization through intermolecular hydrogen bonding, the dihedral angles of the *meso* substituents supporting the hydrogen bond interaction should be smaller than for the free monomer. This decreases the symmetry of the molecule to chiral point group C_2. However, the packing between chiral monomers, in order to avoid strong contacts, must be heterochiral; as show from Gaussian-3 estimations of the structure of H_4TPPS_4 dimers. Using this initial geometry, the data obtained we get the unit cell parameters and the space group. The orientation of porphyrin in the unit cell was adjusted with Cerius2 (Discovery Studio and Visualizer programs; Accelerys). For the refinement five spots on the equator were used. The use of other initial porphyrin geometries, for example that obtained from molecular mechanics (Cerius2 software package; Biosym/Molecular Simulations Inc.) did not led to different final porphyrin packing.

2.3.2. Transmission electron microscopy (TEM) and electron diffraction (ED) measurements.

The aqueous sodium–free solution of H_4TPPS_4 (~1 mM), obtained as previously described,[18b] exhibit tape-like aggregates that grow in length with time.[12b] In order to get optimal samples for the ED studies, the solutions were aged in the fridge for more than one month so as to increase the H_4TPPS_4 aggregation and the length of the homoassociates. The material used for TEM and ED analysis was composed by particles of a thickness of only 3.8 nm (bilayers according to the results presented here; see Results and Discussion). In some cases, ED obtained better spot resolution than X-ray diffraction. However, owing to the impossibility to know whether or not the sample is exactly orthogonal or not to the electron beam, the analysis of the crystal space group was performed with the X-ray data and the electron diffraction data was only for confirming the *h*,*k*,l parameters. Examples of the obtained diagrams are show in Supplementary Information.

2.3.2.1. ED from Oriented Aggregates. The samples for the ED microscopy were disposed on carbon or carbon/Au coated Au grids, which were shadowed with Pt-carbon at an angle of 15° for bright field observations. The deposition was performed by upper contact (30 s) of the grid with the surface of a drop (50 µl) placed on a flat Parafilm® film. The grid with

the absorbed material was washed three times with 0.05 M H_2SO_4 droplets. The samples for internal calibration were Au shadowed perpendicularly [(d111) 0.235 nm]. The samples for bright field observation were shadowed with Pt-carbon at an angle of 15°.

A Philips TECNAI 10 electron microscope was operated at 80 and 100 kV for bright field and electron diffraction modes, respectively.

A difficulty on the interpretation of these ED data, performed in Barcelona, was the lack of a good correlation between the single particle orientation observed in TEM images and the ED data.

2.3.2.2. ED from Single Particles. The H_4TPPS_4 J-aggregate solutions were diluted with water (1:10) just before use in order to minimize the presence of bundles of aggregates while still yielding long aggregates. The dilution was performed by adding 20 μL of H_4TPPS_4 (~1 mM) aged solution in 180 μL H_2O. Notice that it has been previously reported that the aggregation of H_4TPPS_4 may depend on the order of addition.[3] 5 μL of the H_4TPPS_4 solution (~0.1 mM) was deposited on ultrathin (≤ 3 nm) lacey carbon films with holes from 0.25 μm to 5 μm in size (SPI, TED PELLA) supported by a 400 mesh copper grid. After 10 min the drop was sucked with filter paper. With this sample support, the material covering the holes can be imaged by TEM without interferences from the carbon film.

TEM images and electron diffraction patterns were acquired in Berkely using a JEOL 2100-F field emission TEM/STEM instrument operated at 120 kV and equipped with a high angle annular dark field (HAADF) detector. Data acquisition was performed using Gatan software, consisting of a Digital Micrograph, Digiscan II scanning controls and 2K x 2K Ultrascan 1000FT camera. The procedure used is based on the methodology, recently reported,[20] developed for the study of organic molecules highly sensitive to beam damage (see ref.[20] for more details). The procedure is briefly described below.

After performing the standard alignment in TEM mode, some images of each of the studied specimens were taken. Afterwards, the instrument was switched to scanning transmission electron microscopy (STEM) mode selecting a 0.2 nm probe size. A 10 μm condenser aperture (the smallest one) was inserted and centred and after a proper alignment, the parameters for this convergent beam were stored in memory. This setup was used to select the sample area of interest (obtaining high resolution high angle annular dark field HAADF STEM images). On the other hand, a small parallel beam (90 nm) was obtained by adjusting the voltage of the third condenser lens using the Free-Lens Control. The camera length was optimized to get the projection of the back focal plane in the CCD camera used to record the electron diffraction patterns (obtaining low resolution HAADF STEM images). The parameters for the optimized parallel beam to get electron diffraction were also stored in memory. The storage of the optimized parameters for both the parallel and convergent beam allows a fast switching between both imaging modes. The diffraction pattern is rotated 14.5 degrees clockwise with respect to the image (calibrated with InP nanowires as described in ref.[20]) and the camera length was calibrated with a Si(011) standard.

Notice that the single particle ED allows the correlation between the particle alignment observed by TEM and the ED data.

3. Results and discussion

3.1. Monomer constitution and geometry in the J-aggregate

The building unit of H_4TPPS_4 J-aggregates is the porphyrin diprotonated at the pyrroleninic nitrogen atoms but also with four anionic sulfonato groups, i.e. a double zwitterion in a double negatively charged molecule. At pH = 2, and in the absence of aggregation, this is the only species present in the solution,[19b] taking into consideration the pK_a values of the porphyrin NHs and those of the sulfonato groups, and the concentration of protons in the solution (pH ≥ 2).[§] Notice that this also applies to the rest of porphyrins of Scheme 1, but the total charge of the molecule changes to -1 (H_4TPPS_3 and $H_4TPPF_5S_3$) and 0 (H_4TPPS_{2o}).

A reasonable geometry of the zwitterion can be extrapolated from the previously reported crystal X-ray crystal structures of *meso*-tetraphenylporphine (H_4TPP) and other non water-soluble diprotonated porphyrins.[21] In the diprotonated porphyrin the *meso*-aryl/porphine dihedral angles are lower than those of the free base porphyrin as a consequence of the resonance between the *para*-sulfonato group and the positively charged porphyrin ring. Therefore, diprotonation leads to a more planar and compact structure favouring the intermolecular interactions of the "non-covalent polymerization" leading to the J-aggregates. The diprotonation of the porphyrin leads to a ring conformation with the opposite NH bonds above and below the porphyrin plane. The sign of the aryl dihedral angle corresponds to the *syn* conformation between the *orto* CH groups and the NH of the nearby pyrrole rings. In addition, the adjacent *meso*-phenyl substituents show dihedral angles of opposite sign in the more stable conformer (D_{2d} for H_4TPP)[21] and, as inferred by us from Gaussian-3 calculations [UHF, 6-311G(d) basis],[19] S_4 for H_4TPPS_4 for the most stable conformation of the sulfonato groups. The S_4 point group for H_4TPPS_4 corresponds to the most stable conformation of the sulfonato groups, however, in the J-aggregate the sulfonato group conformation can reduce the symmetry order to C_{2v} and even to chiral C_2. Notice that a different axial ordering along the two pairs of opposite *meso*-aryl substituents would lead to different absolute values of the corresponding dihedral angles and, consequently, to the reduction of the symmetry order to a chiral point group.

The intermolecular interactions that stabilize the zwitterion are: (i) electrostatic between the positive charge ring and the anionic sulfonato groups, (ii) hydrogen bonds between NH and SO_3^- groups and, (iii) hydrophobic interactions between non-polar regions, i.e. those of the porphyrin ring and of the *meso*-aryl rings.[22] This has been imagined as a 1d straight chain of zwitterions with the anionic groups at the centre of the neighbouring porphyrin.[22a] Nevertheless, such a structural ordering should be merely understood as a simple graphical description of the driving forces leading to J-aggregates and not as the actual structure of the J- aggregates.

Figure 1. X-ray diffraction image of H_4TPPS_4 J-aggregates and inferred unit cell dimensions (space group $P2_1$ with four porphyrins in the unit cell); *h*,*k*,l parameters for strong, medium, weak and broad spots are shown. The outside ring is the distance control (powder silicon standard, 3.1355 Å). For the comparison of experimental vs calculated distances see Table in Supplementary Information.

3.2. Diffraction data

Fig. 1 shows the best X-ray diffraction diagram leading to the higher *h*,*k*,l parameters that we could obtain (see Supplementary Information for comparison between experimental and calculated distances). Other diagrams of different samples were also coincident with that of Fig. 1. ED patterns show spots in agreement with those of X-ray diffraction (Fig. 2). Different H_4TPPS_4 samples, even if prepared by different synthetic routes, yield J-aggregates showing the same diffraction data. In this respect the ED measurements performed in Barcelona and Berkeley imply different sample preparation, instruments, methodologies and operators.

The observed reflections were indexed, taken into account the systematic absences of *h*,*0*,l, as a primitive monoclinic cell of space group $P2_1$. The *a* side of the unit cell is 29.60 Å, the *b* side 8.40 Å. The *c* side of the unit cell is 28.90 Å, and the β angle 84.99° (Fig. 1). The *b* side of the unit cell corresponds to the hydrogen bond direction of two staking porphyrin molecules. A chiral unit cell is in agreement with recent experimental results pointing to the intrinsic chirality (natural optical activity) of the J-aggregates.[10] The experimental density agrees with the calculated density for a unit cell containing four porphyrin molecules.

This preliminary interpretation was used to model the porphyrin packing within the unit cell. Since the X-ray diagram contained few reflections, all the intermolecular contacts of the model obtained were also refined. Small variation on porphyrin coordinate used in the assessment of the packing in the unit cell have a small effect on the resulting packing of such a large molecule (≈ 2.0 nm in its longer dimension). This was confirmed because the calculation of the packing of four porphyrins in one unit cell using different geometries (standard geometry obtained from molecular

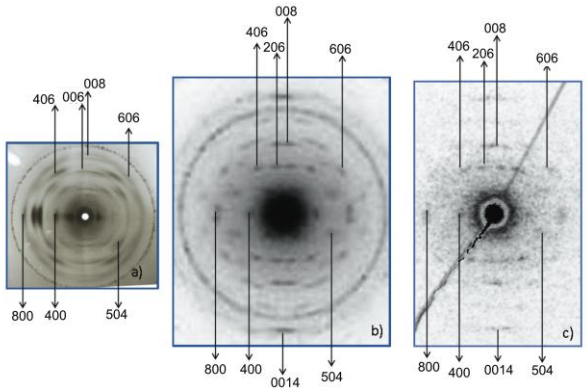

Figure 2. Diffraction patterns of oriented H_4TPPS_4 J-aggregates. Left) X-ray diffraction pattern of an oriented macroscopic film (Fig. 1) Middle) ED pattern of a single particle of unknown orientation (internal control Au 2.35 Å). Right) ED pattern of a single particle of defined orientation [see in Supplementary Information an example of the correlation between particle alignment (TEM) and ED]. The comparison between X-ray and ED data shows the same distances and *h*,*k*,l parameters.

mechanics and geometry obtained from *ab initio* calculations) leads to the same porphyrin packing structure.

The porphyrin arrangement in the unit cell shows a disposition of porphyrin molecules parallel to the *ac* crystallographic plane. This orientation is also characterized by the alignment of the sulphur atoms of each molecule along the *a* direction. Neighbouring molecules related by the binary screw axis are shifted by *b*/2 along the *b* crystallographic direction. An important structural pattern, assumed in all previous reports on these J-aggregates, is the intermolecular interaction between $-SO_3^-$ and NH groups that stabilize the zwitterionic porphyrin.[22g] The resulting structure shows O - N distances (3.0 Å – 3.5 Å) as expected for hydrogen bonds. Porphyrin and aryl rings are approximately parallel to the direction of hydrogen bonding in the pleated sheets. However, two types of dimeric hydrogen bond interactions arise, one formed by parallel porphyrins and another between tilted porphyrins. For the "parallel" dimer the packing between the two H_4TPPS_4 units occurs when the two overlapping phenyl rings show dihedral angles of different sign. This not only leads to a better overlapping of the aromatic rings but also minimizes the steric hindrance between aryl groups and the HC=HC of the nearby pyrrole ring. In the case of the dimeric association between non-parallel porphyrins this constriction is not necessary. All this, together with the symmetry conditions of the crystal space group, renders the stereochemistry of the porphyrin units (see below). The inferred structure shows, in addition to these zwiterionic interactions, ionic interactions between the lateral sulfonato groups and the corresponding counter cations.

3.2.1. Ideal structure of the J-aggregates

Figs. 3 and 4 show the ideal crystal architecture (see below for a discussion on the sites showing more structural disorder) of a set of unit cells in the section of the *ac* plane. The two overlapped porphyrins, in alternate up/down way, determine the unit cell length along the *b* axis (Fig. 3). The superposition of unit cells on the *b* axis shows that the structural motif

yielding the intermolecular stabilization of the zwitterions occurs along the plane perpendicular to the *ac* plane that contains its longest diagonal, i.e. the direction [$\bar{1}$01]. Fig. 3 shows the crystal architecture on the section of the plane direction [$\bar{1}$01]. This sheet interacts laterally with similar layers through ionic interactions between the lateral sulfonato groups (Fig. 3). The two negative charges excess for H_4TPPS_4 molecule requires the presence of a ionic network, between the planes [$\bar{1}$01], implying the lateral anionic sulfonato groups and the corresponding countercations (here corresponding to undetected hydrated protons).

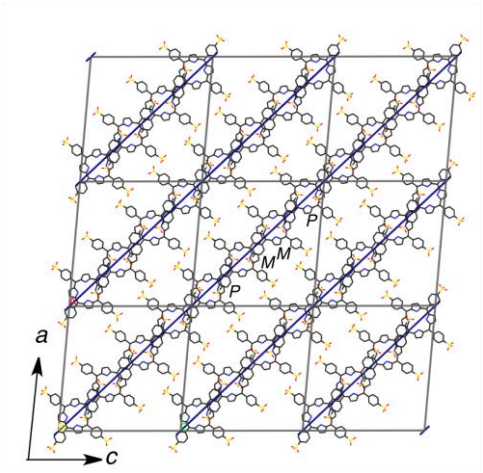

Figure 3. Image of the structural arrangement of 9 unit cells on the *ac* plane (β = 84.99 °; *c* horizontal axis). The blue lines on the longest axis of the *ac* plane of the unit cell is on the intersection with [$\bar{1}$01] (perpendicular to the *ac* plane) that contains the porphyrin architecture responsible for the intermolecular stabilization of the porphyrin zwitterions. The porphyrin packing in the zwitterion intermolecular stabilization locks the conformational enantiomerism as indicated in the central unit cell (see note¶ for the definition of the P and M chirality sign).

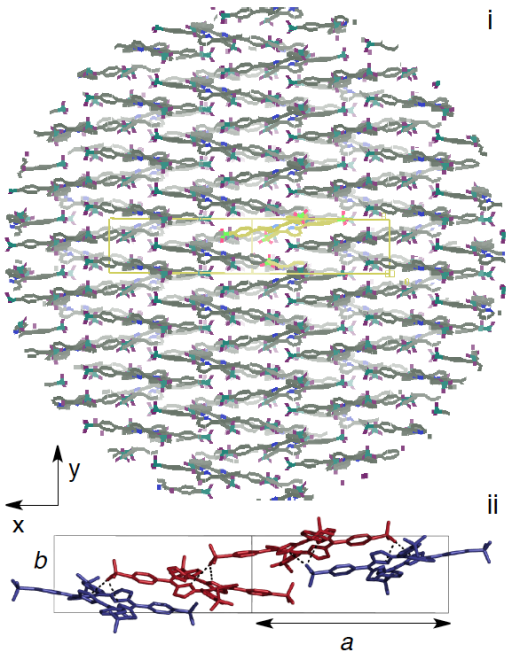

Figure 4. a) Image on [$\bar{1}$01]; y axis coincides with *b* axis and axis x with the direction of the longest diagonal of *ac* (see Fig. 3). b) Detailed image showing the different intermolecular hydrogen bonds (dotted lines O---N) between parallel and tilted dimers (see text and figure in Supplementary Information): the blue and red colours apply respectively for the *P* and *M* conformational enantiomers (see note¶).

A significant structural trend is that the zwittterion intermolecular stabilization, between sulfonato anions and cationic porphyrin rings, do not follows a perfect straight alignment but it diverges from a linear or planar ordering. Each porphyrin is slightly rotated in the same direction around the *b* axis (Fig. 3, the rotation is of opposite direction in each enantiomorph). Furthermore, this is not the only structural aspect that decreases the symmetry order in the structure on the plane [$\bar{1}$01]; Fig. 4 shows that the porphyrin ring is almost perpendicular to the plane [$\bar{1}$01] but somehow inclined with respect to the *b* axis (≈ ± 12°) and that this angle changes its sign each two porphyrins. This leads to π-stacks of parallel dimers showing an angle of alternating sign.‖ Notice that the parallel dimer packing is composed by fixed conformational enantiomers (*P* or *M*, see note¶ for the P and M definition used here) but in racemic composition (P–M). However, the hydrogen bond interaction between tilted porphryins in a homochiral dimer (for example; P–M··M–P in the enantiomorph shown in Figs. 3-4, see also Supplementary Information) and as a consequence the composition of the chiral crystal corresponds to the racemic composition of locked conformational enantiomers.

The structure of the porphyrin arrangement in a plane < $\bar{1}$01> is schematized in Fig. 5. The most significant point is that such a mosaic-like porphyrin architecture, although showing a racemic composition of conformational enantiomers, is already chiral. The chirality arises from the bent arrangement between parallel dimers and the porphyrin slight rotation around the *b* axis. This rotation minimizes the steric hindrance between the 4-sulfonatophenyl group Supplementary the hydrogen bond and the pyrrole HC=CH unit tilted towards the same face. This rotation is transmitted and amplified leading to the absolute configuration ordering shown in Fig 3 for the represented enantiomorph.

3.2.2. Actual structure of H_4TPPS_4 J-aggregates.

The diffraction diagrams, for example those displayed in Fig. 1 and 2, exhibit a diffraction pattern that obviously corresponds to a diffuse structure and not to a regular crystal, but shows a strong texture of the sample, with a clear alignment. However, the structural disorder occurs at defined sites that do not affect the discussed architecture. Structural disorder is observed for *h,k,*l parameters implying S atoms, where small distance changes lead to the obtention of diffuse spots. This indicates that the structural disorder occurs principally between [$\bar{1}$01] layers but also on the [$\bar{1}$01] layer itself.

Most structural disorder takes place in the interaction between $[\bar{1}01]$ layers, i.e. at the ionic network that determines the formation of a layered structure. Surely the 2d ionic

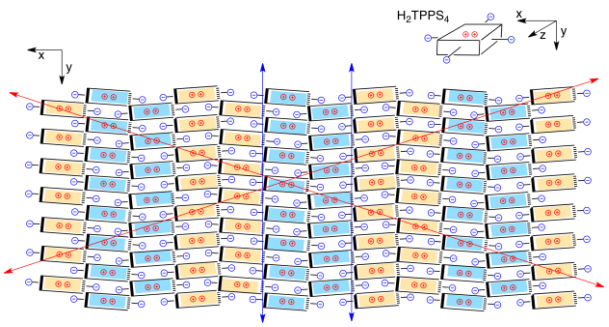

Figure 5. Porphyrin architecture on a plane $<\bar{1}01>$. The sheet is intrinsically chiral. The porphyrin colors indicate the relative configuration of the conformational enantiomers forming the sheet. The assumed excitons are shown by the double arrows; H-exciton, blue trace: J-exciton, red trace).

network between $[\bar{1}01]$ layers does not achieve a significant Madelung energy. Due to the broad arcs observed, a second significant disorder occurs in the $[\bar{1}01]$ layer indicating a non-planar surface; for example *h,k,*l parameters (600), (700), (406), (003) and (004). The plane direction $[\bar{1}01]$ shows slight curvatures above and below of an ideal flat structure, suggesting a flexibility for such a sheet. A non-perfect flat structure implies the transmission of structural disorder to the interlayer architecture, and consequently disorder is detected affecting both intra- and interlayer *h,k,*l parameters: (006), (109), (208), (303), (414) and (804).

The flexibility of the structure on the $[\bar{1}01]$ plane is significant with respect to previous reports on the experiments about selection of the chirality sign in this type of J-aggregates, i.e. the chiral bias that takes place at the critical nucleation point by effect of the hydrodynamic torques of simple strirring.[12]

Structural disorder is observed for *h,k,*l parameters implying S atoms, where small distance changes lead to the obtention of diffuse spots. This indicates that the structural disorder occurs principally between $[\bar{1}01]$ layers but also on the $[\bar{1}01]$ layer.

3.3. Excitonic spectra of the $[\bar{1}01]$ sheet architecture.

The formation of multilayers of sheets with this structure on the plane $[\bar{1}01]$ must have a very low effect on the electronic properties compared to those that are already consequence of the internal structure of the single sheet. This can be easily explained taking into account the type of bond (ionic) and the long distance between layers (≈ 2 nm). Therefore, we can reasonable assume that the electronic and optical properties of the J-aggregates are those determined by the excitons present on the porphyrin sheet of the $[\bar{1}01]$ plane.

Within the sheet on the $[\bar{1}01]$ plane, each porphyrin dimer with parallel arrangement shows couplings in three different directions (Fig. 5): two degenerate J-bands and one H-band. This is in agreement with the simultaneous detection of H- and J-bands. Furthermore, this structure on the $[\bar{1}01]$ plane can be achieved for all porphyrins of Scheme 1 (see discussion below), what explains the similar absorption spectra for all their J-aggregates.

At relatively short distances all three excitonic bands have parallel degenerated excitonic bands. This may explain the bisignated character of the CD signals and the anisotropy changes at different stages of the hierarchical J-aggregation. More work is in progress to calculate the chiral exciton coupling in a structure like the one in Fig. 5.

The angle between H- and J-bands is > 45° (≈ 80°) and the vectorial component of the two degenerated J-bands is perpendicular to the H-bands. This architecture is in agreement with previous reports on polarized fluorescence[5] and on the relative orientation of the linear dichroism at 420 nm and 490 nm measured in oriented particles of the aggregates.[6]

The linear dichroic measurements performed in mature particles show that the H-band is aligned along the longer particle axis[**] (see Supplementary Information), in agreement with the present diffraction data. This corresponds to the general behaviour of aromatic organic compounds, showing a faster crystal growth along the π-stacking direction. In contrast, polarized fluorescence shows that the J-band is aligned along the long axis of the J-aggregate.[5] This is only an apparent contradiction because the fluorescence of the J-aggregates should be assigned to small J-aggregates, probably monolayers, because big J-aggregate particles are expected to yield a lower fluorescence intensity. It is reasonable to assume that the small J-aggregates would be only stable for a minimum length of the zwitterion stabilization along the J-exciton directions, while bigger particles would show a faster growth along the π-stacking (H-axis) direction.

In the first stages of the growth process the maximum decoherence length of the three excitons would be achieved at different stages depending on the preferential direction of growth (Fig. 6). This is in agreement with previous reports showing that during the first aggregation stages the blue-shifted H-band at ≈ 420 nm appears later than the red-shifted J-bands at ≈ 490 nm and ≈ 705 nm. Furthermore, recent results on $H_4TPPF_5S_3$ show that, under specific conditions, at the first stages of the aggregation less red-shifted bands than the final J-band are detected, which correspond to the homoassociation of a low number of porphyrin units.[11] These "oligomeric" bands show resonance light scattering (RLS) spectra (Supplementary Information), that can only be explained if they belong to a big set of degenerated oscillators, as it is the case of the "incomplete" sheets shown in Fig. 6. Notice that at the first stages of the J-aggregate growth, one J-band can be above and the other one below the maximum decoherence length (see Fig. 6). Previous reports point to an autocatalytic/template process in the growth of the first formed aggregates, probably implying a hexameric unit.[11,23] A mechanism of cluster-to-monomer growth implying the formation of smaller sheets from a big one, as it is shown in Fig. 6, could explain such a autocatalytic/template process.

In summary, the sheet structure in the $[\bar{1}01]$ gives a reasonable description of the electronic spectra of the aggregates of all the porphyrins of Scheme 1 and also accounts for the absorption spectra at different stages of the hierarchical growth.

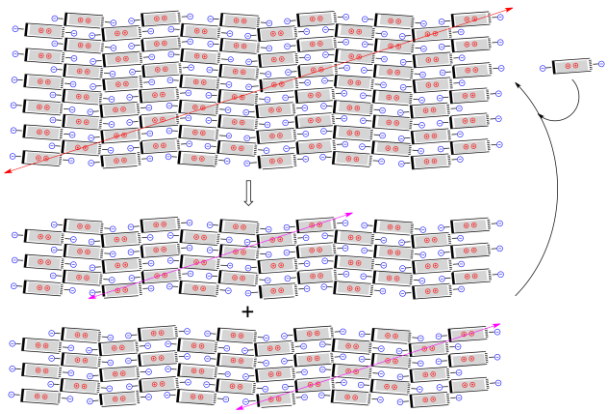

Figure 6. Scheme for an explanation of the autocatalysis/template effects (refs.[10,23]) through the breaking of large sheet $<\bar{1}01>$ to ribbons that would act of templates for monomers and clusters. The scheme indicates how for small aggregates the two J-bands show different excitonic lengths.

3.4. Morphological differences arising from different *meso*-substitution in the porphyrin building block.

The diffraction data indicates that in the ATM/AFM measurements the $[\bar{1}01]$ plane must be parallel to the substrate with the porphyrin units approximately perpendicular to the substrate plane. Then, the porphyrins contact a flat substrate by the lateral sulfonato groups of one side of the $[\bar{1}01]$ plane. With respect to the plane of the substrate, the porphyrins are inclined from the perpendicular axis to the substrate (≈ 10°), so that the J-aggregate ribbons show thicknesses of 1.9 nm (≈ 19.7 nm x cos 10°) for a monolayer, 3.8 nm for a bilayer, and 3.8 + n 1.9 nm for a multilayered particle (2 + n layers). This values is in agreement with previous reports on measurements by AFM in tapping mode, which we have re-examined using state-of-art instrumentation.[#,24]

The H_4TPPS_4 J-aggregates obtained at pH = 2 show a thickness of 3.8 nm which corresponds to a bilayer. Furthermore, in some particles the thickness of 1.8 nm - 1,9 nm corresponding to the monolayer could be detected at the particle edges (see the example in Supplementary Information). No significant differences in thickness could be detected for particles obtained from the porphyrin tetrasodium salts[25] compared to those described here containing hydrated protons at the existing ionic interface between sheets.

There are contradictory reports on the shape of H_4TPPS_4 J-aggregates: monolayered nanotubes[15] *vs* bilayered and multilayered compact tapes. The results presented herein give a reasonable explanation for this fact. To the best of our knowledge the reports on bilayered and multilayered structures correspond to aggregations performed at pH values ≥ 2. In contrast, the reports claiming the detection of nanotubes were performed at lower pH values (pH ≤ 1). In high acidic solutions the lateral sulfonato anion substituents are protonated to sulfonic acid groups and, therefore, unable to form the ionic interface leading to bilayered and multilayered structures. Therefore, when the experimental conditions enable to obtain long enough monolayers of J-aggregates in the J-band direction, the closure into a nanotube of the high flexible $<\bar{1}01>$ monolayer may be possible.

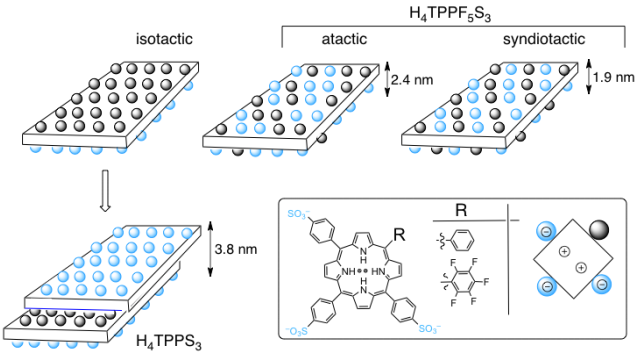

Figure 7. The stereochemistry of the basic architecture on the plane $[\bar{1}01]$, in the cases of H_4TPPS_3 and $H_4TPPF_5S_3$, justifies the formation of mono or bilayered structures depending on the relative configuration of the lateral *meso*-substituents.

The other porphyrins of Scheme 1, because of their lateral *meso*-substituents, may build hydrophobic interfaces between the *meso*-phenyl substituents. Therefore, they can form either monolayers or layered systems through the hydrophobic interactions between the lateral hydrophobic *meso*-substituents. In the case of H_4TPPS_{2o} the symmetric lateral *meso*-substitution allows the formation of multilayered structures by hydrophobic interaction between the lateral phenyl substituents. This is supported by a previous AFM report describing these J-aggregates as relatively thick plates with terraces of monolayer steps.[25] In the case of H_4TPPS_3 and $H_4TPPF_5S_3$ their J-aggregates can show diastereomeric structures (Fig. 7). Only the isotactic configuration would allow the hydrophobic interactions leading to a bilayer: atactic and syndiotactic configurations would not form bilayers. According to previous reports, H_4TPPS_3 shows principally bilayered particles (≈ 3.8 nm),[12b,25] whereas in $H_4TPPF_5S_3$ bilayered structures (≈ 3.9 nm) are very rare and the predominant particles show a thickness corresponding to a monolayer. In the latter case, depending on the preparation procedure, two different thicknesses (1.9 nm and 2.1 nm) have been detected. These distances were attributed to the existence of different stereosisomers, probably to the isotactic and atactic configurations respectively.[11] Notice that the difference between H_4TPPS_3 and $H_4TPPF_5S_3$ regarding whether they lead to bilayers or monolayers is related to the relative stability of their iso- and syndiotactic configurations. In the case of $H_4TPPF_5S_3$, because of dipolar and quadripolar interactions between the pentafluorophenyl substituents, the isotactic configuration is probably less stable than the syndiotactic one.

4. Concluding remarks

The natural optical activity of the aggregates of the achiral porphyrins of Scheme 1 is justified by the intrinsic chirality of the structure that is already present in the formation of simple monolayers. The results suggest that supramolecular helical structures in J-aggregates of achiral building blocks is a transmission towards a higher size scale of an intrinsically chiral packing.

The basic structure of these J-aggregates corresponds to a chiral porphyrin mosaic sheet (Fig. 4). This 2d architecture supported on a plane $< \bar{1}01>$ justifies the simultaneous presence of excitonic H- and J-bands as well as the existence of natural optical activity. Furthermore, it also helps to understand how autocatalysis/template effects can occur at the first stages of the aggregation process.

The existence of the basic 2d structure together with its possibility, or impossibility, to form multilayered structures through interactions of their lateral *meso*-substituents explains why the same absorption spectra are shown by morphologically different J-aggregates (monolayers, bilayers, and multilayers) even when obtained from different *meso*-substituted porphyrins.

It is worth to notice that the case of achiral compounds yielding enantiopure crystals as the more stable mesomorph is a currently hot topic because such crystallizations can be driven to scalemic mixtures of high enantiomeric excesses[8] and new experiments are being reported on the deracemization of racemic conglomerates.[26] These results, together with previous reports on the detection of chirality in J-aggregates,[1b] suggest that in the case of chiral soft-matter deviations from the racemic composition are more easily obtained than in the case of crystallizations. This is probably due to the relatively different rates between the primary and the secondary nucleation stages compared to those of crystallization processes.

Previous reports on the chiral sign selection by effect of hydrodynamic torques on H_4TPPS_3 J-aggregates, according to the present results, must be explained by the action of flows on clusters during the primary nucleation stage. The present results point to that a torque in the bifurcation point (transition from achiral, or fast-racemizing, sheet-like clusters to the chiral 2d-structure in the plane $[\bar{1}01]$) would select the corresponding enantiomorph at the critical nucleation stage. The elasticity of such a sheet, manifested also in the diffraction data by the sites showing structural disorder, should be taken into account for the explanation of the previous reversible changes on the circular optical polarization properties by effect of hydrodynamic torques.[6,7b,c,27]

Notes and references

[a] *Department of Organic Chemistry, Institute of Cosmos Science, University of Barcelona (IECC-UB), c. Martí i Franquès 1. Barcelona, Catalonia, 08028-Spain. jmribo@ub.edu. A.S Present address; Department of Chemistry, Faculty of Sciences, Universitat Autònoma de Barcelona, Bellaterra, Catalonia, 08193-Spain.*

[b] *Materials Sciences Division, Lawrence Berkeley National Laboratory, Berkeley, CA 94720, United States. Present address; Alba Synchrotron Light Source, Carretera BP 1413, Km. 3.3, Cerdanyola del Vallès, Catalonia, Barcelona, 08290-Spain.*

[b] *Materials Sciences Division, Lawrence Berkeley National Laboratory, Berkeley, CA 94720, United States. Present address; Alba Synchrotron Light Source, Carretera BP 1413, Km. 3.3, Cerdanyola del Vallès, Catalonia, Barcelona, 08290-Spain.*

[c] *Department of Chemical Engineering, Polytechnic University of Catalonia (UPC), Av. Diagonal 647, Catalonia, Barcelona, 08028-Spain.*

[c] *The Molecular Foundry, Lawrence Berkeley National Laboratory, Berkeley, California 94720, United States.*

[d] *Nanometric Techniques Unit. Scientific and Technological Services (CCiTUB), University of Barcelona, c. Lluís Solé i Sabarís 1-3, Catalonia, Barcelona, 08028-Spain.*

† Electronic Supplementary Information (ESI) available: Experimental and calculated distances from the diffraction data and additional image of the crystal structure; TEM images and TEM diffraction images; RLS spectra; Optical polarization properties spectra; AFM images. See DOI: 10.1039/b000000x/

‡ A chiral shaped nano structure, when the chiral shape is not an expression of the intrinsically chirality of the matter structure cannot show natural optical activity.[14] Notice, that in the case of a metal helix or of a helical cholesteric ordering, the electronic ordering is described of a intrinsically chiral polariton/soliton.

§ Aggregation at higher pH values, for example pH = 4, occurs in the presence of free-base porphyrin and this may interfere with the homoassociation process of the diprotonated species. Aggregation at pH ≤ 1 leads to protonation of sulfonato groups of the J-aggregates; see discussion in the text.

¶ *P* and *M* chirality on the units of the porphyrin sheet is here defined by the axial chirality given by the two lateral, opposite, *meso*-aryl substitutents.

|| It is surely significant that exhaust drying (for example by lyophilization) leads to disaggregation but not to the monomer (434 nm); a species absorbing at 455 nm is formed that has been attributed to a dimer.[19a]

** Our previous report of ref.[6] (first column, third paragraph of p. 1689) is an erroneous interpretation of the physical definition of the light polarization alignment in respect to the laboratory coordinates (see Supplementary Information).

Our previous reports of refs.[12b,25] correspond to lower thickness values than those reported here and in ref.[11]. However these more recent measurements were performed in modern probe instruments (see Materials and Methods) which can use one tenth of the force used in older instruments in tapping mode, and thus effects due to the elasticity of the J-aggregates[12b] disappear and a more exact measure of this parameter becomes possible.[24]

1 a) T. Kobayashi, *J-Aggregates*; World Scientific: Singapore, 1996. b) S. Kirstein and S. Dähne, *Int. J. Photoenergy* 2006, **5**, 3. c) F. Würthner, T. E. Kaiser and C. R Saha-Möller, *Angew. Chem. Int. Ed.* 2011, **50**, 3376.

2 a) T. S. Balaban, H. Tamiaki and A. R. Holzwarth (Würthner F., Ed), *Topics Current Chemistry* 2005, **258**, 1-38. b) S. T. Balaban, *Acc. Chem. Res.* 2005, **62**, 612. c) A. Satake and Y. Kobuke, *Org. Biomol. Chem.* 2007, **5**, 1679.

3 a) M. A. Castriciano, A. Romeo, V. Villari, N. Micali and L. Monsù Scolaro, *J. Phys. Chem.* 2003, **107**, 8765. b) C. Escudero, A. D'Urso, R. Lauceri, C. Bonaccorso, D. Sciottob, S. Di Bellab, Z. El-Hachemi, J. Crusats, J. M: Ribó and R. Purrello, *J. Porphyrins Phthalocyanines* 2010, **14**, 708. b) A. D'Urso, M. E. Fragala and R, Purrello, *Chem. Commun.* 2012, **48**, 8156.

4 W. Cooper, *Chem. Phys. Lett.* 1970, **7**, 73.

5 a) O. Ohno, Y. Kaizu and H. Kobayashi, *J. Chem. Phys.* 1993, **99**, 4128. b) R. Rubires, J. Crusats, Z. El-Hachemi, T. Jaramillo, M. Lopez M, E. Valls, J.-A. Farrera and J. M. Ribo, *New J. Chem.* 1999, **23**, 189. c) H. Matsuzava, H. Kobayashi and T. Maeda, *Bull. Chem. Soc. Jpn.* 2012, **85**, 774.

6 O. Arteaga, C. Escudero, G. Oncins, Z. El-Hachemi, J. Llorens, J. Crusats, A. Canillas and J. M. Ribo, *Chem. Asian J.* 2009, **4**, 1687.

7 a) Z. El-Hachemi, O. Arteaga, A. Canillas, J. Crusats, C. Escudero, R. Kuroda, T. Harada, M. Rosa and J. M. Ribo, *Chem. Eur. J.* 2008, **14**, 6438. b) O. Arteaga, A. Canillas, R. Purrello and J. M. Ribo, *Opt. Lett.* 2009, **34**, 2177. c) O. Arteaga, A. Canillas, J.

Crusats, Z. El-Hachemi, J. Llorens, E. Sacristan and J.M. Ribo, *ChemPhysChem* 2010, **11**, 3511.

8 a) E. Havinga, *Biochim. Biophys. Acta* 1954, **13**, 171. b) D. K: Kondepudi, R. Kaufman and N. Singh, Science 1990, **250**, 975 . c) J. M. McBride and R. L. Carter, *Angew. Chem. Int. Ed.* 1991, **30**, 293. d) D. K. Kondepudi and K. Asakura, *Acc. Chem. Res.* 2001, 34, 946 – 954.

9 De Greef T. F. A.; Smulders M. M. J.; Wolffs M.; Schenning A. P. H. J.; Sijbesma R. P.; Meijer E. W. *Chem. Rev.* **2009**, *109*, 5687-5754.

10 A. Sorrenti, Z. El-Hachemi, O. Arteaga, A. Canillas, J. Crusats and J. M. Ribo, *Chem. Eur. J.* 2012, **18**, 8820

11 A. Sorrenti, Z. El-Hachemi, J. Crusats and J.M. Ribo, *Chem Commun*. 2011, **47**, 8551.

12 a) J. M. Ribo, J. Crusats, F. Sagues, J. Claret and R. Rubires, *Science* 2001, **292**, 2063. b) C. Escudero, J. Crusats, I. Diez-Perez, Z. El-Hachemi and J. M. Ribo, *Angew. Chem. Int. Ed*. 2006, **45**, 8032. c) N. Micali, H. Engelkamp, P. G. van Rhee, P. C. M. Christianen, L. Monsù Scolaro and L. J. C Maan, *Nature Chemistry* 2012, **4**, 201.

13 a) C. Spitz and S. Dähne, *J. Phys. Chem. B* 2000, **104**, 8664. b) U. De Rossi, S. Dähne, S. C. J. Mesker and H. P. J. M. Dekkers, *Angew. Chem. Int. Ed.* 2003, **35**, 760.

14 a) P. Curie, *J. de Physique* 1894, **3**, 393. b) J. Earman *J. Intert. Stud. Philos. Sci.* 2004, **18**, 173.

15 a) R. Rotomkis, R. Augulis, V. Snitka, R. Valiokas and B. Liedberg, *J. Phys. Chem B* 2004, **108**, 2833. b) S. C. Gandini, E. L. Gelamo, R. Itri and M. Tabak, *Biophys. J.* 2003, **85**, 1259. c) S. M. Vlaming, R. Augulis, M. C. A. Stuart, J. Knoester and P. H. M. van Loosdrecht, *J. Chem. Phys. B* 2009, **113**, 2273.

16 R. F. Pasternack, *Ann New York Acad Sci.* 1973, **206**, 614.

17 M. De Napoli, S. Nardis, R. Paolesse, M. G. H. Vicente, R. Lauceri and R. Purrello, *J. Am. Chem. Soc.* 2004, **126**, 5934.

18 a) J. M. Ribo, R. Rubires, Z. El-Hachemi, J.-A. Farrera, L. Campos, G. L. Pakhomov and M. Vendrell, *Mater. Sci. Eng. C* 2000, **11**,107. b) C. Escudero, Z. El-Hachemi, J. Crusats and J. M. Ribo, *J. Porphyrins Phthalyanines* 2005, **9**, 852-863.

19 J. M. Frisch, G. W. Trucks, H. B. G. Schlegel, E. Scuseria, M. A. Robb, J. R. Cheeseman, J. A. Montgomery Jr., T. Vreven, K. N. Kudin, J. C. Burant, J. M. Millam, S. S. Iyengar, J. Tomasi, V. Barone, B. Mennucci, M. Cossi, G. Scalmani, N. Rega, G. A. Petersson, H. Nakatsuji, M. Hada, M. Ehara, K. Toyota, R. Fukuda, J. Hasegawa, M. Ishida, T. Nakajima, Y. Honda, O. Kitao, H. Nakai, M. Klene, X. Li, J. E. Knox, H. P. Hratchian, J. B. Cross, V. Bakken, C. Adamo, J. Jaramillo, R. Gomperts, R. E. Stratmann, O. Yazyev, A. J. Austin, R. Cammi, C. Pomelli, J. Ochterski, P. Y. Ayala, K. Morokuma, G. A. Voth, P. Salvador, J. J. Dannenberg, V. G. Zakrzewski, S. Dapprich, A. D. Daniels, M. C. Strain, O. Farkas, D. K. Malick, A. D. Rabuck, K. Raghavachari, J. B. Foresman, J. V. Ortiz, Q. Cui, A. G. Baboul, S. Clifford, J. Cioslowski, B. B. Stefanov, G. Liu, A. Liashenko, P. Piskorz, I. Komaromi, R. L. Martin, D. J. Fox, T. Keith, M. A. Al-Laham, C. Y. Peng, A. Nanayakkara, M. Challacombe, P. M. W. Gill, B. G. Johnson, W. Chen, M. W. Wong, C. Gonzalez and J. A. Pople, GAUSSIAN 03 (Revision C.02), Gaussian, Inc., Wallingford, CT, 2004.Gaussian-3.

20 V.Altoe, F. Martin, A. Katan, M. Salmeron and S.Aloni, *Nano Letters* 2012, **12**, 1295.

21 a) M. J. Hamor, T. A. Hamor and J. L. Hoard, *J. Am. Chem. Soc.* 1964, **86**, 1938. b) A. Stone and E. B. Fleischer, *J. Am. Chem. Soc.* 1968, **90**, 2735. c) coordinate files TPHPOR10 and TPPPPFEC, Cambridge Data Base: F. H. Allen, O. Kennard and R. Taylor, *Acc. Chem. Res.* 1983, **16**, 146.

22 a) J. M. Ribó, J. Crusats, J.-A. Farrera and M. L. Valero, *J.C.S. Chem. Commun.* 1994, 681. b) N. C. Maiti, S. Mazumdar, N. Periasamy, *J. Phys. Chem. B* 1998, **102**, 1528. c) S. C. M. Gandini, V. E. Yushmanov, I. E. Borissevitch and M. Tabak, *Langmuir* 1999, **15**, 6233. d) P. Kubát, K. Lang, K. Procházková and P. Anzenbacher Jr., *Langmuir* 2003, **19**. 422. e) L. Zhang, M. Liu, *J. Phys. Chem* B 2009, **113**, 4015. f) A. L. Yeats, A. D. Schwab, B. Massare, D. E. Johnston, A. T. Johnson, J. C. de Paula and W. Smith, *J. Phys. Chem. C* 2008 **112**, 2170. g) M. Rahmad and H. J. Harmon, *J. Porphyrins Phthalocyanines* 2007, **11**, 125.

23 R. F. Pasternack, C. Fleming, S. Herring, P. J. Collings and J. de Paula, *Biophys. J.* 2000, **79**, 550.

24 A. Sikora and L. Bednarz, *Meas. Sci. Technol*. 2011, **22**, 094005(8).

25 J. Crusats, J. Claret, I. Díez-Pérez, Z. El-Hachemi, H. García-Ortega, R. Rubires, F. Sagués and J. M. Ribó, *Chem. Commun.* 2003, **39**, 1588.

26 a) C. Viedma, *Phys. Rev. Lett.* 2005, **94**, 065504. b) J. Crusats, S. Veintemillas-Verdaguer and J. M. Ribo, *Chem. Eur. J.* 2006, **12**, 7776. c) W. L. Noorduin, T. Izumi, A. Millemaggi, M. Leeman, H. Meekens, W. J. P. van Enckevort, R. M. Kellogg, B. Kaptein, E. Vlieg and D. G. Blackmond, *J. Am. Chem. Soc.* 2008, **130**, 1158.

27 A. D'Urso, R. Randazzo, L. LoFaro and R. Purrello, *Angew. Chem. Int. Ed.* 2010, **49**, 108.